SUPPORTING INFORMATION

Experimental setup

Figure S1 shows a sketch of the experimental setup used for the quantum dot (QD) quantum frequency conversion (QFC) experiment. The QD-micropillar source is placed inside a closed-cycle cryostat operating at 10 K, where the QD is excited in its p-shell at 903.31 nm (measured on a wavemeter) by a tunable Ti-Sapphire cw laser. The photons are collected through a high numerical aperture objective (NA = 0.75, 100x) that sits within the cryostat, enabling high efficiency collection of emitted photons [48]. A half-wave plate (HWP) enables selection of the laser polarization incident on the sample, and an output polarizer (pol.) in the detection path can select for a specific

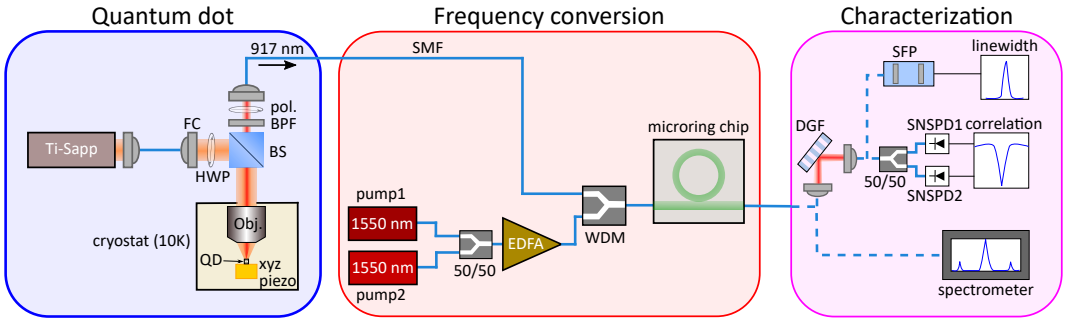

FIG. S1. The experimental setup consists of the QD source in a closed-cycle cryostat at 10 K and the frequency converter chip is in a separate room-temperature setup. The QD single photons before and after frequency conversion are characterized through a grating spectrometer, intensity autocorrelation using a time-correlated single photon counting (TCSPC) module, and scanning Fabry-Perot cavity for the linewidth measurement. FC: Fiber coupler, BPF: Band-pass filter, HWP: half-wave plate, BS: Beam splitter, pol: polarizer, SMF: Single-mode fiber, EDFA: Erbium-doped fiber amplifier, WDM: Wavelength division multiplexer, DGF: Diffraction grating filter, SNSPD: Superconducting nanowire single photon detector, SFP: Scanning Fabry-Perot.

emission polarization and help suppress laser scatter. A narrow (1 nm) band-pass filter separates the excitation from the emission, which is coupled to a single-mode fiber (SMF) and sent to the frequency converter chip in a separate room-temperature setup. The frequency converter chip is temperature-tuned to match its nearest cavity mode with the QD emission. The two 1550 nm pumps are combined in a 50/50 coupler and sent to an erbium-doped fiber amplifier (EDFA) to generate required total pump power ($\approx$ 20 mW on the chip). The QD signal and amplified pumps are combined by a wavelength division multiplexer (WDM), and injected into the microring access waveguide through a lensed fiber. The frequency-converted signals are collected through another lensed fiber at the access waveguide output. The converted signal can be directly coupled to a grating spectrometer for spectral analysis, or into a ruled reflective diffraction grating optical setup of bandwidth $\approx$ 150 GHz (efficiency $\approx$ 50 %) to spectrally select the blue-shifted idler from the frequency-converted spectrum. We use a standard Hanbury-Brown and Twiss setup to measure the intensity autocorrelation of the QD emission before and after frequency conversion, where photons are detected using superconducting nanowire single photon detectors (SNSPDs) operating in a 0.7 K cryostat. The linewidth of the signal and idler is measured using a separate setup based on a scanning Fabry-Perot cavity with free-spectral range of $\approx$ 40 GHz and linewidth of $\approx$ 200 MHz.

Fabrication of the Micropillar Quantum Dot Source

The QD sample consists a single layer of low density InAs QDs grown via molecular beam epitaxy and located at the center of a λ-thick GaAs cavity surrounded by two $Al_{0.9}Ga_{0.1}As$/ GaAs Bragg mirrors with 12 (25) pairs. The density of self-assembled InAs quantum dots varies continuously along the wafer by stopping the rotation of the substrate during InAs deposition.

The first step in fabrication of the micropillar cavities is location of the QDs using a photoluminescence-based positioning technique [49]. Next, the sample is spin-coated with a negative tone electron beam resist (HSQ FOx15). The resist is exposed using an electron-beam lithography system at 100 keV. After the exposure and development processes, the mask pattern is transferred into the sample via an inductively-coupled plasma reactive ion etching system.

Estimation of conversion efficiency

The conversion efficiency of the blue idler is estimated from the experimental measurements in two ways, using spectrometer data and through photon counting. In case of the spectrometer measurements, we integrate the area under the peak of the QD input signal and the frequency-converted blue idler (see Fig. 3a,b of main text) to obtain the total counts before and after conversion. The QD input signal spectrum (Fig. 3a) is obtained after spectrally filtering the excitation laser through a grating filter (transmission efficiency of $\approx$ 50 %, Figure S1), whereas the grating filter is bypassed during the conversion measurement (i.e., the QD signal is sent directly to the converter

chip). The spectrum after conversion is obtained by directly sending the converted signal to the spectrometer without any spectral filtering (Fig. 3b). Accounting for the differences in filtering and the chip transmission efficiency of ≈ 15 %, the on-chip conversion efficiency for the blue idler comes out to be 12.8 % $\pm$ 1.8 %, where the uncertainty is a one standard deviation value that arises from the spread in chip coupling losses and transmission of the grating filter, as well as fluctuations in the measured spectrometer count rates. For photon counting, we spectrally filter both the QD signal and blue idler before sending them to the SNSPDs. The photon counts are recorded during the intensity autocorrelation measurements. The conversion efficiency of the blue idler in this case is found to be 11.4 % $\pm$1.6 %, where the uncertainty is a one standard deviation value that arises from the spread in chip coupling losses and transmission of the grating filter, as well as fluctuations in the count rates measured by the SNSPDs. The conversion efficiency value for the two cases are similar to within the measurement uncertainties, and match the theoretically predicted value as shown in Fig. 4c.

Analysis of Intensity Autocorrelation data

We use a standard Hanbury-Brown and Twiss setup to obtain the second-order correlation function $g^{(2)}(\tau)$ of the QD signal before and after frequency conversion, where τ is the time delay between detection events on the two SNSPD (Fig S1). We record histograms of delays between detection events using a time-correlated single photon counting (TCSPC) module with 128 ps resolution. For sufficiently small τ, the histogram of coincidences is equivalent to $g^{(2)}(\tau)$, see [50]. The normalized histogram under cw excitation is fitted by a double-exponential function:

$$\mathrm{g}^{(2)}(\tau) = 1 + A_1 \exp(-\gamma_1 \cdot |\tau|) + A_2 \exp(-\gamma_2 \cdot |\tau|)$$

with $A_1 + A_2 = -1$. This form is expected for a two-level system coupled to a single dark state, and describes antibunching at $\tau = 0$, bunching at some later time delay, and a return to the Poissonian level at $\tau \to \infty$ [51]. The fits shown in Fig. 3c,d of the main text are obtained using a nonlinear least squares procedure (for the pulsed pumping data, only the raw data is presented and no fit is performed). In all cases, the $g^{(2)}(0)$ value is taken as the measured data point at zero time delay and not the fit value. For the error in the $g^{(2)}(0)$ values, we calculate the fluctuation in the coincidence counts in the histograms for $\tau \gg 0$ (i.e., the Poissonian level), and propagate the error.

Fabrication of the Microring Frequency Converter

Microrings are fabricated in a 500 nm thick Si_3N_4 layer on top of a 3 μm thick SiO_2 layer. The Si_3N_4 layer was created by low-pressure chemical vapour deposition while the SiO_2 layer was grown via thermal oxidation of a 100 mm Si wafer. The wavelength-dependent refractive index and thickness of the layers were determined using a spectroscopic ellipsometer, with the data fit to an extended Sellmeier model. After cleaving into chips, the microring-waveguide devices were created by electron-beam lithography of a negative tone resist, followed by reactive ion etching of the Si_3N_4 using a CF_4/CHF_3 chemistry, removal of deposited polymer and remnant resist, and annealing at 1150 °C in an O_2 environment for 3 h. The microring used in our experiments has radius of 40 μm and a ring width of 1450 nm.

Frequency converter design summary

While four-wave-mixing Bragg scattering (FWM-BS) has been demonstrated in optical fibers in several experiments (e.g., [38, 39], it has only recently been demonstrated in integrated microresonators [37]. We qualitatively review the design approach for these devices here, and summarize some of the salient features with respect to the quantum dot quantum frequency conversion experiments that are the focus of this work.

FWM-BS uses two non-degenerate pumps at frequencies ω_{p1} and ω_{p2} to spectrally shift an input signal at ω_s to output idlers, one of which is blue-shifted with respect to the signal, that is, $\omega_{i+} = \omega_s + |\omega_{p1} - \omega_{p2}|$, and the other which is red-shifted with respect to the signal, $\omega_{i-} = \omega_s - |\omega_{p1} - \omega_{p2}|$. Like any other $\chi^{(3)}$ parametric nonlinear optical process [52], efficient operation means that these energy conservation relationships need to be accompanied by momentum conservation, or phase-matching, so that $\beta_{i+} = \beta_s + |\beta_{p1} - \beta_{p2}|$ and $\beta_{i-} = \beta_s - |\beta_{p1} - \beta_{p2}|$, where β_k is the propagation constant of light at frequency ω_k. $\beta_k = 2\pi n_{\mathrm{eff},k}/\lambda_k$, where $n_{\mathrm{eff},k}$ is the effective refractive index at wavelength λ_k. $n_{\mathrm{eff},k}$ is a wavelength-dependent quantity influenced by different factors, including the material

refractive indices of the waveguide layers and the effects of geometric confinement. In most cases in which FWM-BS has been studied in optical fibers [36, 38, 53–55], the dispersion of the fibers was such that only one of the two possible idlers could be both frequency- and phase-matched, so that only a single idler needed to be considered. In cases in which the pumps are relatively close to each other spectrally, however, both up- and down-shifted idlers can satisfy these criteria [56], so that the conversion efficiency into each idler can be approximately equal.

We use the microring geometry to provide resonant enhancement of the FWM-BS process, enabling efficient conversion to be achieved for ten mW-scale, continuous wave pumps [37]. The phase-matching criterion $\beta_{i\pm} = \beta_s \pm |\beta_{p1} - \beta_{p2}|$ becomes $m_{i\pm} = m_s \pm |m_{p1} - m_{p2}|$, where m_k is the azimuthal mode number of the cavity mode in the relevant band (signal, idler, pump 1, or pump 2). While finding a set of whispering gallery modes that satisfies this relationship is straightforward, one then needs the corresponding mode frequencies to satisfy the energy conservation relationship $\omega_{i\pm} = \omega_s \pm |\omega_{p1} - \omega_{p2}|$, which will not be true for an arbitrary resonator cross-section. As described in Ref. [37], we can satisfy this frequency matching requirement by looking for resonators that have equal free-spectral ranges in the two wavelength bands (pumps in the 1550 nm band and signal/idler in the 920 nm band). For our devices, this prescription leads to relatively weak dispersion in the two wavelength bands. This enables a large number of mode combinations to be phase- and frequency-matched, providing significant flexibility in the operation of the frequency converter, as described in Fig. 5 in the main text. In particular, this weak dispersion is the key that allows efficient conversion for both a wide range of signal wavelengths and a tunable spectral translation range (Fig. 5a,b in the main text).

Modeling of the Microring Frequency Converter and Its Efficiency

Modeling of the FWM-BS process in microrings was developed in Ref. [37]; see also Ref. [57]. The most general approach that considers both FWM-BS and any competing four-wave-mixing processes is that based on numerical simulation of the Lugiato-Lefever equation, as discussed in [37]. While such an approach accounts for the higher-order idlers we observe in experiment, the basic behavior of the system, for example the conversion efficiency into the first-order idlers, can be well-described by a simplified coupled mode theory that considers a restricted basis of modes. Here, we first outline this theory, before describing how we apply it to photons emitted from single QDs, so that we can calculate the conversion efficiency as a function of input signal linewidth as shown in Fig. 4c of the main text. We also consider how, if the input signal linewidth is fixed, the loaded linewidth of the frequency conversion ring can be adjusted to improve conversion efficiency.

We start with the coupled mode equations [37]:

$$t_R \frac{dE_s}{dt} = -(\alpha + i\delta_s)E_s + i\Omega_0 E_{i-} + i\Omega_0 E_{i+} + i\sqrt{\theta P_s}, \tag{S1}$$

$$t_R \frac{dE_{i+}}{dt} = -\left(\alpha + i(\delta_s + \Omega_1 + \Omega_2)\right) E_{i+} + i\Omega_0 E_s, \tag{S2}$$

$$t_R \frac{dE_{i-}}{dt} = -\left(\alpha + i(\delta_s - \Omega_1 + \Omega_2)\right) E_{i-} + i\Omega_0 E_s, \tag{S3}$$

where $E_{s,i\pm}$ are the intracavity mean fields corresponding to the signal and two adjacent idlers ($|E|^2$ representing the average power traveling inside the cavity), t_R is the round-trip time, α is the cavity loss rate in the 930 nm band ($\alpha = \hat{\omega}_s t_R/(2Q_L)$ with $\hat{\omega}_s$ and Q_L being the signal resonance frequency and its loaded Q, respectively), δ_s denotes the signal detuning, θ is the power coupling coefficient between the resonator and the access waveguide ($\theta = \hat{\omega}_s t_R/Q_c$ with Q_c being the coupling Q), and P_s represents the power of a cw signal. The parameters $\Omega_n (n = 0, 1, 2)$ are defined as:

$$\Omega_0 \equiv 2\gamma_s L |E_{p1} E_{p2}|, \tag{S4}$$

$$\Omega_1 \equiv \frac{\delta_{i+} - \delta_{i-}}{2}, \tag{S5}$$

$$\Omega_2 \equiv \frac{\delta_{i+} + \delta_{i-} - 2\delta_s}{2}, \tag{S6}$$

where γ_s is the Kerr nonlinear coefficient in the 930 nm band, L is circumference of the microring resonator ($L \equiv 2\pi R$ with R being the ring radius), $E_{p1,p2}$ denote the intracavity mean fields of the two pumps in the 1550 nm band, and

$\delta_{i\pm}$ are the detunings of the two idlers. A straightforward calculation shows that $\Omega_{1,2}$ can be expressed as:

$$\Omega_1 \approx \left(D_1|\mu| - |\omega_{p1} - \omega_{p2}|\right) t_R - \frac{\gamma_p L}{2}\left(|E_{p1}|^2 - |E_{p2}|^2\right), \tag{S7}$$

$$\Omega_2 \approx \frac{1}{2} D_2 \mu^2 t_R, \tag{S8}$$

where γ_p is the Kerr nonlinear coefficient in the 1550 nm band. In our configuration, we use two pumps with equal power, thus Ω_1 (Eq. S7) is determined by the difference in frequency of the pump lasers ($|\omega_{p1} - \omega_{p2}|$) and the FSR in the 930 nm band (D_1).

The above set of equations serves as a convenient tool for us to simulate the on-chip conversion efficiency for both the cw and pulsed input signal. First, for the cw case we can simply calculate the steady-state solution of the intracavity fields such as $E_{i\pm}$ for a given signal power and detuning. The corresponding power of the idlers in the waveguide is calculated based on input-output relations, which are subsequently normalized by the input signal power to give the on-chip conversion efficiency. Next, for the pulsed input, the signal is decomposed into a series of cw components through Fourier analysis. The spectrum of the converted idler can then be obtained by solving the steady-state idler fields for each cw component. The conversion efficiency in this case is defined as the averaged idler photon flux normalized by the averaged signal photon flux.

We now consider the case in which the loaded linewidth of the microring frequency converter is a free parameter, with a fixed intrinsic quality factor (Q) of 1.6×10^6. In practice, the loaded linewidth can be varied by tailoring the access waveguide coupling design. We consider the conversion efficiency for input signals with two different linewidths, the 2.87 GHz linewidth we measure for our existing QD single-photon source, and a 1.0 GHz linewidth that has been achieved for many QD single-photon sources reported in the literature (the transform-limited linewidth for a system with a 1 ns lifetime is $\approx$ 160 MHz). For a fixed input signal linewidth, the conversion efficiency increases with the converter bandwidth (Fig. S2), at a relatively fast rate up until the point at which the microring resonator loaded linewidth is a factor of two or three times larger than that of the input signal, and then slowly thereafter until the conversion efficiency saturates. For the QD studied in the main text, the conversion efficiency can increase from the 12 % we measure to $\approx$30 %, if the microresonator loaded linewidth is increased by about a factor of four, to $\approx$4.5 GHz. This will primarily come at the expense of the pump power required for efficient conversion, assuming that the loaded quality factors in the 1550 nm pump band are correspondingly reduced (we note that it may be possible to engineer the waveguide coupling so that only the input signal and output idler resonances have 4.5 GHz linewidths, while the 1550 nm pump resonances remain close to critically coupled at their narrower linewidths). On the other hand, for the 1 GHz linewidth QD, a modest increase in loaded linewidth to 2 GHz would result in a 30 % conversion efficiency.

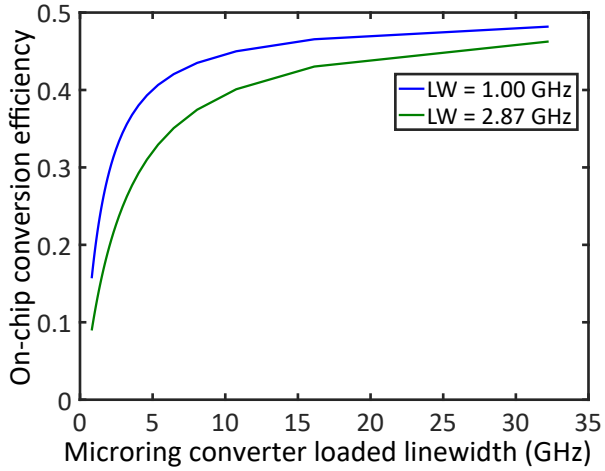

FIG. S2. Simulated conversion efficiency for increasing microring frequency converter loaded linewidth for fixed input signal linewidth (LW) of 1 GHz (blue) and 2.87 GHz (green). The green curve represents the linewidth of the QD studied in the main text.

Frequency converter noise

The 1550 nm pumps used in our frequency converter induce added noise in the 917 nm band, resulting in degradation in the $g^{(2)}(0)$ values as observed in Fig. 3 in the main text. In this section, we further quantify this on-chip noise flux and its effect on the performance of QD single-photon sources.

For a total on-chip pump power of 20 mW, we measure an on-chip noise flux in the blue-shifted idler band of 3.2 fW $\pm$ 0.1 fW, where the one standard deviation uncertainty is due to variation in the chip insertion loss. This corresponds to an on-chip noise photon flux of 1.5×10^4 s^{-1}, which as mentioned in the main text, is uniformly distributed in time. For scenarios in which the QD is operated under pulsed excitation, this can be converted to a number of noise photons per excitation pulse. At an 80 MHz repetition rate and assuming a 2 ns time bin (consistent with containing the full wavepacket of a QD single photon), this corresponds to 3×10^{-5} noise photons per pulse. A QD single-photon source which not only has a high source brightness but efficient coupling to the frequency converter chip might be expected to generate at least 0.01 photons per pulse (on-chip), resulting in a signal-to-noise level in excess of 30 (with a maximum value of 3×10^3) at 10 % conversion efficiency. Moreover, as noted in the main text, we operate at a relatively high pump power to broaden the converter bandwidth, due to the relatively broad linewidth photons our QD source generates. At a pump power of 10 mW, the same conversion efficiency can be achieved if the source linewidth is sufficiently narrow, with the noise flux reduced by about a factor of 2.5.

To provide some additional perspective on the added noise, we measure its spectrum in the converted idler channel using a scanning Fabry-Perot (SFP) resonator, as discussed in the main text. The QD signal is disconnected from the converter chip while the pumps remain on, and the added noise signal is measured (after the bandpass grating filter that initially selects this spectral channel), using the same conditions as the blue idler bandwidth measurement. The resulting spectrum of the added noise is plotted alongside the spectrum of the converted blue idler in Fig. S3, and exhibits a signal-to-noise ratio of more than 10. We note that if sufficiently narrow linewidth input photons sources are used (e.g., from a QD source exhibiting indistinguishable photons or other lifetime-limited quantum emitters such as vacancy centers in diamond or single alkali atoms), additional spectral filtering within the microcavity frequency converter bandwidth can provide improved noise performance.

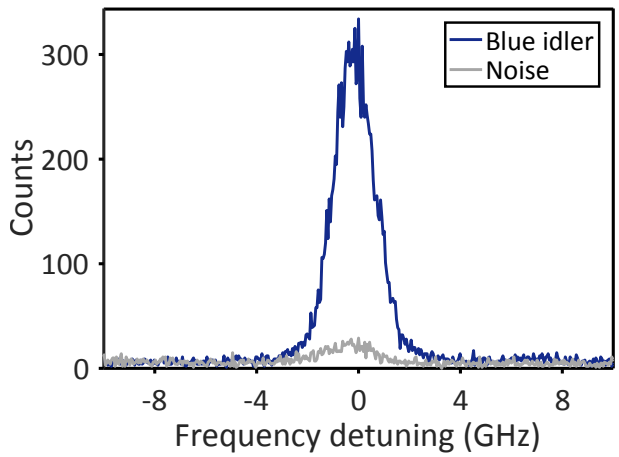

FIG. S3. Scanning Fabry-Perot measurement of the converted blue idler (blue) and the converter noise (grey) in the same channel. The noise is measured in absence of the input QD signal.

Optimizing the frequency converter efficiency

Here, we discuss the factors affecting the conversion efficiency and its optimum limit. There are essentially three factors that are limiting conversion efficiency. First, both the blue-shifted and red-shifted idlers are created with roughly equal conversion efficiency, as they are both equally well phase- and frequency-matched (though this balance can be slightly adjusted by tuning the pump spectral positions). From Fig. 4a (main text), we can precisely add up the conversion efficiency for the two idlers in the experiment, which would be 31 % (blue-shifted) + 26 % (red-shifted) = 57 %. Next, we have conversion into higher-order idlers. From Fig. 4a, conversion into higher order idlers adds

up to about 16 %. Therefore, the total conversion efficiency into all idlers (first order red- and blue-detuned plus all higher order idlers) is about 73 %.

Finally, we need to take into account the level of waveguide-resonator coupling, that is, the requirement that (ideally) all input photons be coupled into the microring resonator, and all frequency-converted output photons be coupled out of the microring. Our microring's total loaded linewidth is $\approx$ 1.1 GHz, of which $\approx$ 200 MHz represents the intrinsic linewidth and the remaining 900 MHz is due to coupling to the access waveguide. On the extraction side, this corresponds to out-coupling about 82 % of the frequency-converted photons from the ring into the access waveguide. The 73 % conversion efficiency for all idlers mentioned above could thus be improved to 89 % if perfect overcoupling is achieved.

The above analysis suggests that a conversion efficiency approaching 90 % could be achieved provided that the level of overcoupling is improved, and that only one set of microring modes be phase- and frequency-matched. In practice, this might be possible by using different techniques to mismatch undesired conversion channels (i.e., the red-shifted idler and higher-order idlers). Mode selective gratings and coupled resonators are amongst the approaches that might enable such possibilities.